IEEE Access
Multidisciplinary ⋮ Rapid Review ⋮ Open Access Journal

Received March 26, 2022, accepted April 17, 2022, date of publication April 18, 2022, date of current version April 25, 2022.

Digital Object Identifier 10.1109/ACCESS.2022.3168788

Solution of Nonlinear Reaction-Diffusion Model in Porous Catalysts Arising in Micro-Vessel and Soft Tissue Using a Metaheuristic

ABDUL HAMID GANIE[1], IRFAN UR RAHMAN[2], MUHAMMAD SULAIMAN[2], AND KAMSING NONLAOPON[3]

[1]Basic Science Department, College of Science and Theoretical Studies, Saudi Electronic University, Abha Male 61421, Saudi Arabia
[2]Department of Mathematics, Abdul Wali Khan University Mardan, Mardan 23200, Pakistan
[3]Department of Mathematics, Faculty of Science, Khon Kaen University, Khon Kaen 40002, Thailand

Corresponding author: Kamsing Nonlaopon (nkamsi@kku.ac.th)

ABSTRACT The steady-state reactive transport model (RTM) is a generalization of the nonlinear reaction-diffusion model in porous catalysts. The RTM is expressed as a non-linear ordinary differential equation of second-order with boundary conditions. Artificial neural network (ANN), Particle swarm optimization (PSO), and hybrid of PSO-SQP (Sequential Quadratic Programming) are used to obtain accurate, approximate solutions to the non-linear RTM. The proposed technique is applied to three different cases of non-linear RTM. The properties of the nonlinear reactive transport model in porous catalysts are investigated by considering various cases based on variation in the half-saturation concentration "α" and the characteristic reaction rate "β." The stability, reliability, and exactness of the proposed technique are established through comparison with the outcomes of the standard numerical procedure with the RK4 method and along with the different performance indices, which are Root-Mean-Square Error (RMSE), (TIC), Absolute Error (AE), and Mean Absolute Deviation (MAD).

INDEX TERMS Artificial neural networks, nonlinear reactive transport model, particle swarm optimization, mathematical modeling.

I. INTRODUCTION

Problems arising in microvessels and fluid are multiscale model of nonlinear steady-state one-dimensional reactive transport (RTM) which is also known as reaction-diffusion model in porous catalysts are used to solve those types of problems [1]–[3]. Reactive transport model dynamics are essential for the study of physical and biological processes because they are used to develop behavior in various Earth-related studies [4], [5]. The development of reactive transport models provides a forum for testing and integrating new theoretical information on transport, geochemical, and biological processes. The effect of changes in air transport and temperature, as well as water pollutants, due to diffusion and convection characteristics play an important role in human lives in the reactive transport model phenomenon of heat and mass transfer [6]–[8].

The associate editor coordinating the review of this manuscript and approving it for publication was Vivek Kumar Sehgal.

The reactive transport model, which governs in a one-dimensional steady-state can be stated as follows [9]:

$$\hat{D}\frac{\mathrm{d}^2\theta}{\mathrm{d}X^2} - V\frac{\mathrm{d}\theta}{\mathrm{d}X} - r(\theta) = 0, \quad 0 \le X \le L, \tag{1}$$

with boundary conditions as follows:

$$\theta(L) = \theta_s \text{ and } \frac{\mathrm{d}\theta(0)}{\mathrm{d}X} = 0, \tag{2}$$

the advective velocity is denoted as V, the reaction process is denoted as $r(\theta)$ and the diffusivity parameter is denoted as $\hat{D}$. Moreover the parameters are discussed in [3] and [1] in detail. By using the non-dimensional quantities $\theta(x) = \frac{\theta(X)}{\theta_s}$, $x = \frac{X}{L}$, and the non-dimensional reaction term $r(x)$ into Eq. (1), we get

$$\frac{\mathrm{d}^2\theta}{\mathrm{d}x^2} - P\frac{\mathrm{d}\theta}{\mathrm{d}x} - r(x) = 0, \quad 0 \le x \le 1, \tag{3}$$

where $P = \frac{LV}{\hat{D}}$ is so-called Péclet number. Without advection of transport, we have $P = 0$, and the model was used to study

porous catalyst pellets as a diffusion and reaction model in this case. The $r(x)$ is assumed by Michaelis–Menten [3] to be a nondimensional reaction, then Eq. (4) is modified in the following way:

$$\frac{d^2\theta}{dx^2} - \frac{\beta\theta(x)}{\alpha + \theta(x)} = 0, \quad 0 \le x \le 1, \tag{4}$$

the boundary conditions as:

$$\frac{d\theta(0)}{dx} = 0, \quad \theta(1) = 1, \tag{5}$$

where α, is the concentration of half saturation, which cannot be negative and β is characteristic reaction rate, when $\beta < 0$, then instead of product reactions we looks at the reactives. The RTM problem in Eq. (3) has been extensively studied without advective transport ($P = 0$), whereas the RTM problem in Eqs. (4, 5) is a fluid and solute transport model arising from soft tissue and microvessel research.

The model (3)-(4), which was recently introduced by Ellery and Simpson [3], is a modification of the primer model, referred to as the nonlinear reaction-diffusion model in porous catalysts, which has been used to study porous catalyst pellets and has been analysed using a variety of techniques [10]–[12]. The models (3)-(4) incorporate advective and diffusive transport, as well as the Michaelis-Menten reaction model, which is frequently used to describe biological processes [13]–[15]. This model encapsulates a variety of critical engineering processes, including various applications in chemical [16], [17] and environmental engineering [13], [15]. The boundary value problems (1)–(2) have a nonlinear fractional term, which makes them rather challenging to solve numerically. Ellery and Simpson [3] proposed a Taylor series solution for this model that is actually convergent if the Michaelis-Menten reaction term has finite derivatives.

The RTM problems (4, 5) can be solved for different half-saturation concentration β and characteristic reaction rate α. The RTM's significant role motivates researchers to develop solutions for the model. Alves, Van Genuchten [18], and Torideet [19] provide analytical solutions for steady-state non-linear RTMs, such as the Homotopy analysis method [20], the Adomian decomposition method [21]–[24], and the Taylor–Galerkin methods for non-linear dynamical problems [25]. These RTM investigations use deterministic numerical and analytical methodologies, each with its own set of advantages, applicability, reliability, and limitations. On the other hand, artificial intelligence-based techniques have not yet been investigated for solving mathematical relations of nonlinear RTMs.

The research community has used stochastic numerical techniques based on artificial intelligence algorithms to investigate a wide range of engineering and technology applications [26]–[29]. The most prominent stochastic paradigms applications via the exploitation of ANNs, particle swarm optimization (PSO), swarm intelligence, pattern search (PS) include nonlinear Thomas–Fermi model [30], corneal model [31], multi-phase flow model [32], dynamic model for heart-beat [32], the model of wire coating analysis [32], beam-column Designs model [33], over-current relays model [34], model of plasma [35], Bratu problem [36], Bagley–Torvik models [37] and Riccati model [38].

Additionally, the stochastic algorithms also handled problems arising in electromagnetics [39], astrophysics [40], electrical circuits [41], communication, signal processing, controls [42], plasma physics [43], bio-informatics [44], atomic physics [45], and nanotechnology [42]. These are inspirations for the author to investigate, analyze, and exploit research stochastic mathematical methodologies to establish a new, precise, robust, and dependable computing approach to investigate nonlinear reactive transport models that arise in soft tissue and microvessel studies.

A. SUMMARY OF THE STUDIES

The following is a summary of the study's findings in terms of critical features:

1) For solving nonlinear second-order reactive transport model systems, governing Earth and heat systems, the accurate modeling of ANNs that have been optimized with particle swarm optimization PSO) and PSO-SQP is efficiently exploited.
2) To determine reactive transport model dynamics for various cases based on of variations of the characteristic half-dynamic concentration and reaction rates, the proposed stochastic technique is applied with reasonable accuracy when compared to the RK4 solution. The proposed approach outperforms the other methods in terms of performance.
3) The techniques comparison indicates that the performance of PSO and PSO-SQP is better than the rest of the other numerical techniques for such a model.
4) PSO's high performance in investigating the governing mathematical equations of reactive transport models (RTMs) was further supported by a detailed evaluation of the findings using statistical performance from MAD, TIC, and RMSE.

II. ORGANIZATION OF THE PAPER

The rest of this paper is structured as follows:

Sect. 3: Design is provided with computational intelligence paradigms for the non-linear transport models results.

Sect. 4: Presented the designed scheme of the proposed technique.

Sect. 5: Statistics results are presented on the basis of various tests.

Sect. 6: For the reactive transport model, numerical experiments are illustrated with graphical and numerical diagrams.

Sect. 7: Conclusions and future research directions are discussed.

III. DESIGN METHODOLOGY

The nonlinear reactive transport model (RTMs) design scheme is divided into two parts. The first section describes the system's ANN-based modeling. The second section of

the study provides an overview of the optimization strategies that are employed as dynamic methods for training ANN model weights. The proposed scheme's workflow diagram is visually shown in Fig. 2.

A. MATHEMATICAL MODELING

The non-linear reactive transport model (RTM) mathematical modeling is described in two sections. The first section constructs ANN simulations for the system's solution and derivative terms. The second section discusses the use of ANN simulations to formulate fitness functions.

We create an artificial neural network approximate solution as follows by continuously mapping the solution $\hat{\theta}(x)$ and its derivative up-to n^{th} order as:

$$\hat{\theta}(x) = \sum_{i=1}^{k} \tilde{A}_i f\left(\tilde{\omega}_i x + \tilde{\gamma}_i\right), \tag{6}$$

$$\frac{\mathrm{d}\theta}{\mathrm{d}x} = \sum_{i=1}^{k} \tilde{A}_i \frac{\mathrm{d}}{\mathrm{d}x} f\left(\tilde{\omega}_i x + \tilde{\gamma}_i\right), \tag{7}$$

$$\frac{\mathrm{d}^2\hat{\theta}}{\mathrm{d}x^2} = \sum_{i=1}^{k} \tilde{A}_i \frac{\mathrm{d}^2}{\mathrm{d}x^2} f\left(\tilde{\omega}_i x + \tilde{\gamma}_i\right), \tag{8}$$

$$\frac{\mathrm{d}^n\hat{\theta}}{\mathrm{d}x^n} = \sum_{i=1}^{k} \tilde{A}_i \frac{\mathrm{d}^n}{\mathrm{d}x^n} f\left(\tilde{\omega}_i x + \tilde{\gamma}_i\right). \tag{9}$$

Here adaptive parameters of networks, are $\tilde{\gamma}_i$, $\tilde{A}_i$ and $\bar{\omega}_i$ are in i_{th} form, f is an activation function and k represent total number of neurons. In artificial neural network, log-sigmoid $f(\tau) = 1/\left(1 + e^{-\tau}\right)$, is usually used for activation function, where the $\tau = \tilde{\omega}_i x + \bar{\gamma}_i$.

Using activation function the log-sigmoid in the set of equations from Eq.(6) to Eq.(8) and its derivatives can be represents as follow.

$$\hat{\theta}(x) = \sum_{i=1}^{k} \frac{\tilde{A}_i}{1 + e^{-(\tilde{\omega}_i x + \tilde{\gamma}_i)}}, \tag{10}$$

$$\frac{\mathrm{d}\hat{\theta}}{\mathrm{d}x} = \sum_{i=1}^{k} \frac{\tilde{A}_i \tilde{\omega}_i e^{-\left(\hat{\omega}_i x + \tilde{\gamma}_i\right)}}{\left(1 + e^{-(\tilde{\omega}_i x + \tilde{\gamma}_i)}\right)^2}, \tag{11}$$

$$\frac{\mathrm{d}^2\hat{\theta}}{\mathrm{d}x^2} = \sum_{i=1}^{k} \tilde{A}_i \tilde{\omega}_i^2 \left[\frac{2e^{-2(\tilde{\omega}_i x + \tilde{\gamma}_i)}}{\left(1 + e^{-(\tilde{\omega}_i x + \tilde{\gamma}_i)}\right)^3} - \frac{e^{-(\tilde{\omega}_i x + \tilde{\gamma}_i)}}{\left(1 + e^{-(\tilde{\omega}_i x + \tilde{\gamma}_i)}\right)^2}\right], \tag{12}$$

$$\frac{\mathrm{d}^n\hat{\theta}}{\mathrm{d}x^n} = \sum_{i=1}^{k} \tilde{A}_i \tilde{\omega}_i^n \left[\begin{array}{c} \frac{n! e^{-n(\tilde{\omega}_i x + \tilde{\gamma}_i)}}{\left(1 + e^{-(\tilde{\omega}_i x + \tilde{\gamma}_i)}\right)^{n+1}} \\ -\frac{n(n-1) e^{-(n-1)(\tilde{\omega}_i x + \tilde{\gamma}_i)}}{\left(1 + e^{-(\tilde{\omega}_i x + \tilde{\gamma}_i)}\right)^{n}} + \cdots \\ + \frac{(-1)^{n-1} e^{-(\tilde{\omega}_i x + \tilde{\gamma}_i)}}{\left(1 + e^{-(\tilde{\omega}_i x + \tilde{\gamma}_i)}\right)^{2}} \end{array}\right]. \tag{13}$$

The ANN architecture of RTM is built using the appropriate network combinations described in Eq (4) in the form of single inputs, outputs and hidden layers as indicated in Fig 2.

The RTM fitness function of Eqs (4, 5) is developed using the approximation principle in the mean square sense as:

$$\varepsilon = \varepsilon_1 + \varepsilon_2. \tag{14}$$

Although ε_1 represents the mean square error of the differential equation representing RTM.

$$\varepsilon_1 = \frac{1}{K} \sum_{k=1}^{K} \left(\frac{\mathrm{d}^2\hat{\theta}_k}{\mathrm{d}x^2} - \frac{\alpha\hat{\theta}_k}{\beta + \hat{\theta}_k}\right)^2, \tag{15}$$

and ε_2 is the boundary condition the mean square error as:

$$\varepsilon_2 = \frac{1}{2}\left(\left(\hat{\theta}_k - 1\right)^2 + \left(\frac{\mathrm{d}\hat{\theta}_0}{\mathrm{d}x}\right)^2\right), \tag{16}$$

for $\hat{\theta}_k = \hat{\theta}(x_k)$, $x_k = kh$, $h = 1/k$. The network for $\hat{\theta}_k$ and its first and second-order networks are described in a set of equations from Eqs. (10) to (12). Now, the approximate solution $\hat{\theta}(x)$ will be overlapping with the exact solution $\theta(x)$ of the reactive transport model as defined in Eqs. (4,5), if the tuned weights of the network with $\varepsilon_{\mathrm{RTM}}$ are appropriately close to zero.

IV. LEARNING METHODOLOGY

Once the fitness function for the non-linear reaction-diffusion model has been constructed using an artificial neural network, we applied PSO and PSO-SQP to obtain optimal weights for the model.

A. OPTIMIZATION PROCEDURE

1) PARTICLE SWARM OPTIMIZATION

At the end of the nineteenth century, Eberhart and Kennedy developed PSO, a global heuristic search optimization tool. Particle swarm optimization utilizes genetic algorithms [46] and has become one of the most popular optimization techniques due to its ease of implementation and lower memory requirements [47]. PSO provides improved performance on various standards and the spectrum of engineering issues to provide more optimal results. PSO is associated with the combined swarm success of bird flocking and fish schooling [48]. Multicast communication network routing problems [49], solar photovoltaic systems [50], vehicle-to-grid energy resource scheduling [51], high-dimensional data clustering [52], pathway optimization for humanoid robots [53], multilevel thresholding [54], collective robotic selection, and cancer classification gene selection [55], are some of the most recent PSO applications.

Each candidate outcome is a particle that represents an optimization model in the search space. To form a swarm, randomly generated particles explore the problem in the PSO algorithm. Initial swarms are distributed to determine the technique's optimum efficiency on a larger scale. Each particle in the swarm has fitness values that define the problem's parameters, known as the objective function. An iteratively optimal solution provides parameter initialization in the particle swarm optimization algorithm. The velocity and position

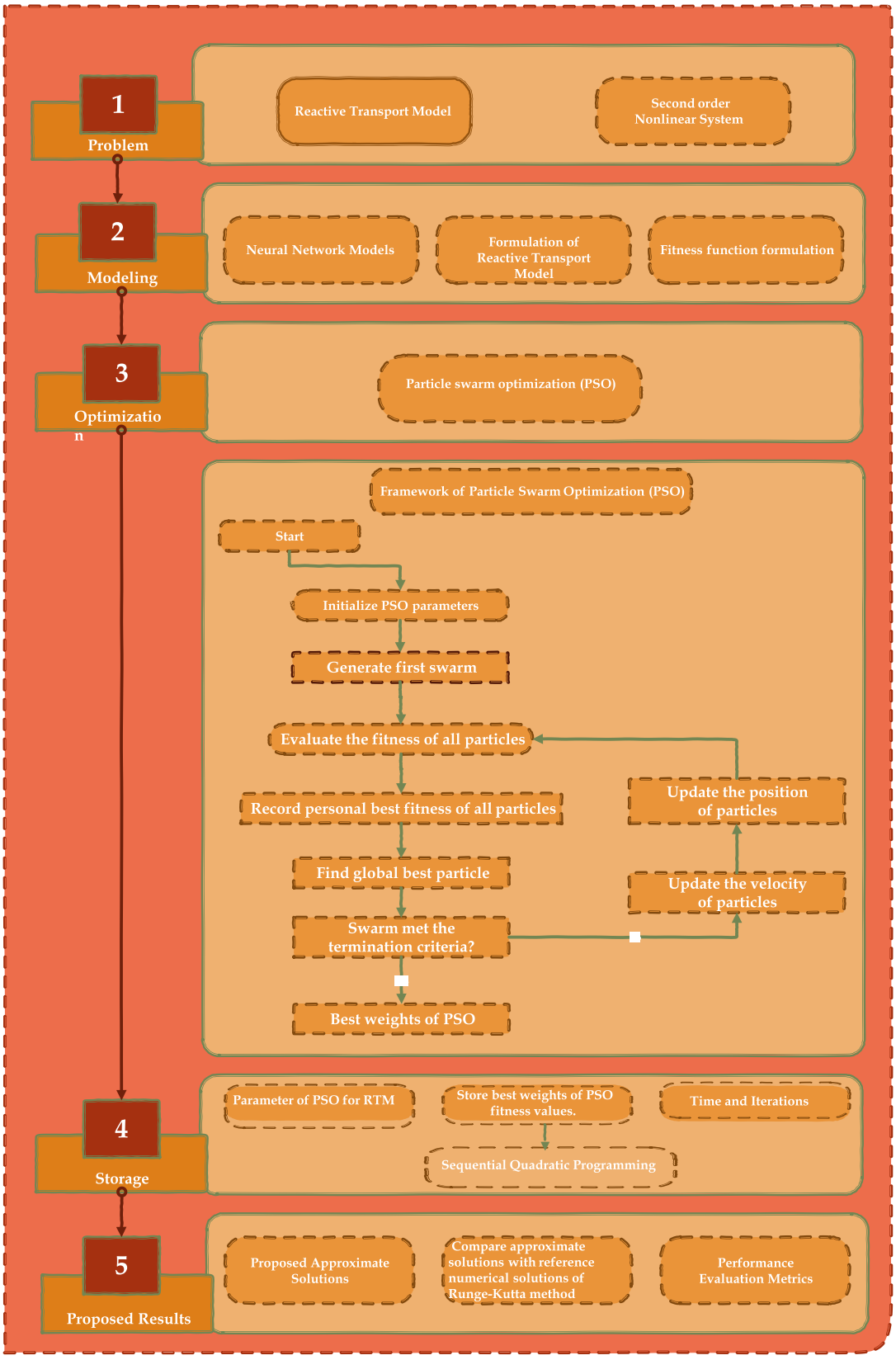

FIGURE 1. Graphical abstract of proposed algorithm.

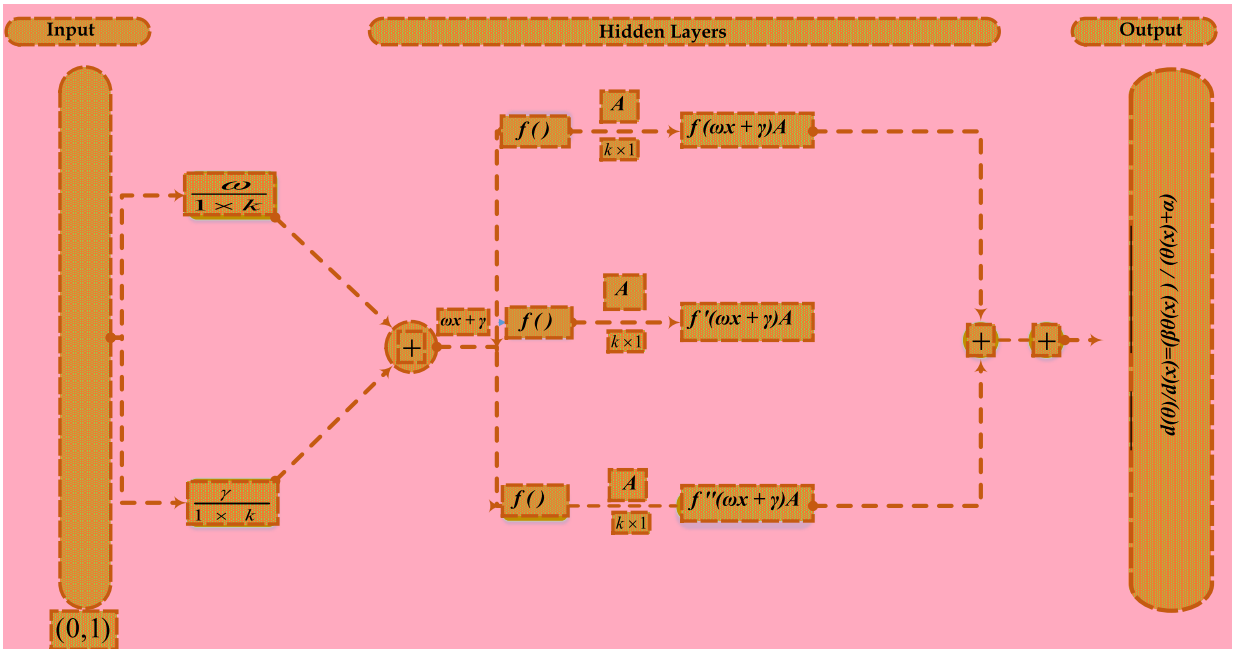

FIGURE 2. ANN architecture for non-linear RTM.

of the swarm are restructured by using the global best and local positions of its previous point, $\boldsymbol{P}_{GB}^{r-1}$ and $\boldsymbol{P}_{LB}^{r-1}$.

The standard continuous velocity and position particle swarm optimization update form is provided as:

$$\boldsymbol{X}_i^r = \boldsymbol{X}_i^{r-1} + \boldsymbol{V}_i^{r-1}, \tag{17}$$

$$\boldsymbol{V}_i^r = \omega \boldsymbol{V}_i^{r-1} + a_1 \boldsymbol{r}_1 \left(\boldsymbol{P}_{LB}^{r-1} - \boldsymbol{X}_i^{r-1}\right) + a_2 \boldsymbol{r}_2 \left(\boldsymbol{P}_{GB}^{r-1} - \boldsymbol{X}_i^{r-1}\right), \tag{18}$$

the velocity vector represented by $\mathbf{V}_i$ and i^{ih} swarm particle denoted by vector $\mathbf{X}_i$. The random vectors is denoted by r_l and r_2, and the acceleration constant denoted by a_l and a_2, where as inertia weight is $\omega \in [0, 1]$. The elements of the velocity vector is between $[-v_{\max}, v_{\max}]$, and maximum velocity is indicated by $v_{\max}$. Based on a predefined number of flights, the output of the algorithm is stopped. The global search performance of PSO is increased further with the use of the Sequential Quadratic Programming method (SQP), which is an efficient, speedy, and fast local search optimization technique.

2) SEQUENTIAL QUADRATIC PROGRAMMING

Sequential quadratic programming (SQP) has become a very reliable, effective, efficient and accurate method for optimizing the linear and nonlinear constrained optimization problems since early 1970s. SQP is the class of optimization algorithms with conceptual procedure of various specific methods that have evolved. The dominance of SQP algorithm is established through computational and theoretical experimentations. SQP algorithm is considered to be one of the fundamental techniques to be exploited in the domain of both public and commercial sector problems of practical significance. Few recent applications addressed effectively by SQP procedures are bilinear optimal control problem [7], finding the worst resonance response [56]. Furthermore, Fletcher [57] and Schittkowski [58] are good sources of reference material on SQP methods. Montoya [59], Kim *et al.* [60], Witkowska and Smierzchalski [61], Kouzoupis [62], and Welhazi [63] are just a few recent examples of how the technique has been applied to engineering or applied science problems.

Using the MATLAB optimization toolbox, the SQP algorithm is used to optimize the artificial neural network model using parameters and initial starting point. Fig. (1) depicts the PSO and PSO-SQP algorithms' workflow, while the pseudocodes for reproducing the results are as follows:

V. PERFORMANCE INDICATORS

The performance of the designed model for solving nonlinear RTM models is examined in this research study by integrating various performance indices, with a focus on mean absolute deviation (MAD), the inequality coefficient of Theil (TIC) and Root Mean Squared Error (RMSE). The benefits of using these three metrics provide an in-depth analysis of precision, stability, and convergence for perfect modeling of different optimal values.

The mathematical output operators for the numerical solution θ_m and the approximate solution $\hat{\theta}_m$ is displayed as:

$$\text{MAD} = \frac{1}{n} \sum_{m=1}^{n} \left| \theta_m - \hat{\theta}_m \right|, \tag{19}$$

TABLE 1. DE's proposed hybrid soft computing technique's pseudo-code.

Particle Swarm Optimization (PSO): `Start`
Initialization:Randomly generate the initial swarm of the particle.
Initialize the parameters in 'PSO'.
Calculation of fitness: Calculate value of the fitness for every particle using Eq. (14).
Ranking: Rank each particle based on minimum function fitness value.
Criteria of Stoppage: Stop the optimization process for any of the following.
(i) Chosen fitness level achieved.
(ii) Number of desired flights/cycles performed.
If stopping criteria are not attained, then move to step 5.
Renewal: Call the position using Eq. (17) and velocity using Eq. (18).
Improvement: The algorithm repeat from step 2 to step 6, until the whole flights is achieved.
Storage: The best fitness values store and represent it the global best particle
End of PSO. If the predefined conditions are met, the SQP will be fed the
optimal PSO weights to produce the desired outcome.
Particle Swarm Optimization (PSO): `End`
Sequential Programming Algorithm: `Start`
Inputs: $W_{PSO_{Best}}$ as initial points of SQP
Output: PSO-SQP weight vector i.e., $W_{PSO-SQP}$
Initialization: Start-Point as $W_{PSO-SQP}$ Iterations, bounds, and other settings are assigned.
Termination: The adaptation process terminates if one or more of the given conditions exists:
'Fitness' equal to or less than 10^{-13}
'Total iterations' equal to or less than 2000
'TolFun' equal to or less than 10^{-18}
'TolX' equal to or less than 10^{-20}
'TolCon' equal to or less than 10^{-18}
'MaxFunEvals' equal to or less than 600,000
while (The termination requirement has been met.)
Fitness evaluation: Evaluate the fitness of each **W**.
Fine-tuning: As a solver for SQP, use 'fmincon'. **W** parameters are updated for each iteration of SQP, and modified fitness is calculated.
Storage: Weights vector saved. $W_{PSO-SQP}$, functions evaluations, fitness value, iterations, and time.
Sequential Programming Algorithm: `End`

where n is a grid point for input. TIC, and RMSE error functions are defined mathematically as:

$$\mathrm{TIC} = \frac{\sqrt{\frac{1}{n}\sum_{m=1}^{n}\left(\theta_m - \hat{\theta}_m\right)^2}}{\left(\sqrt{\frac{1}{n}\sum_{m=1}^{n}\theta_m^2} + \sqrt{\frac{1}{n}\sum_{m=1}^{n}\hat{\theta}_m^2}\right)}, \tag{20}$$

$$\mathrm{RMSE} = \sqrt{\frac{1}{n}\sum_{m=1}^{n}\left(\theta_m - \hat{\theta}_m\right)^2}, \tag{21}$$

Fig. (10) are shown for the graphical illustration of TIC, RMSE, FIT, and MAD of three cases for hundreds of independent runs on a semi-log scale. We also depicted the histograms of TIC, FIT, and MAD for each case. The graphical illustration of the indices fitness values show that most of the values are close to zero which show the robustness and effectiveness of the propose techniques as shown in Figs. (4), (6) and (9).

VI. NUMERICAL RESULTS

The findings of the simulation results are shown here for three scenarios of reactive transport model (RTM) dynamics with variance in the half-saturation concentration denoted by α and the characteristic reaction rate represented by β using intelligent ANN-based computing methods optimized with PSO and PSO-SQP. The graphical illustration of weights is shown in Fig. (8). The approximate solution for all cases by using the optimal wights of the proposed techniques can be written in the form of:

$$\hat{\theta}_{c_n}(t) = \frac{\alpha_1}{1+e^{-(\beta_1 t+\gamma_1)}}\frac{\alpha_2}{1+e^{-(\beta_2 t+\gamma_2)}} + \frac{\alpha_3}{1+e^{-(\beta_3 t+\gamma_3)}} + \frac{\alpha_4}{1+e^{-(\beta_4 t+\gamma_4)}} + \frac{\alpha_5}{1+e^{-(\beta_5 t+\gamma_5)}} + \frac{\alpha_6}{1+e^{-(\beta_6 t+\gamma_6)}} + \frac{\alpha_7}{1+e^{-(\beta_7 t+\gamma_7)}} + \frac{\alpha_8}{1+e^{-(\beta_8 t+\gamma_8)}} + \frac{\alpha_9}{1+e^{-(\beta_9 t+\gamma_9)}} + \frac{\alpha_{10}}{1+e^{-(\beta_{10} t+\gamma_{10})}}. \tag{22}$$

A. CASE-I: $\beta = 0.5$ AND $\alpha = 0.2$

The reactive transport model (RTM) Eqs. (4,5) may be stated as follows in this case [9]:

$$\frac{\mathrm{d}^2\theta}{\mathrm{d}x^2} - \frac{(0.5)\theta(x)}{(0.2)+\theta(x)} = 0, \tag{23}$$

subject to the boundary conditions

$$\frac{\mathrm{d}\theta}{\mathrm{d}x} = 0, \quad \theta(1) = 1. \tag{24}$$

The fitness function ε, for case 1 can be expressed as:

$$\varepsilon = \frac{1}{10}\sum_{k=1}^{10}\left(\frac{\mathrm{d}^2\hat{\theta}_k}{\mathrm{d}x^2} - \frac{0.5\hat{\theta}_k}{0.2+\hat{\theta}_k}\right)^2 + \frac{1}{2}\left(\left(\hat{\theta}_K - 1\right)^2 + \left(\frac{\mathrm{d}\hat{\theta}_0}{\mathrm{d}x}\right)^2\right). \tag{25}$$

Particle Swarm Optimization and Sequential Quadratic Programming is applied for optimizing the fitness function (25). In Eq. (22), the optimal weights of PSO and PSO-SQP are used to find the approximate solutions for case 2 of the reactive transport model as shown in Eq. (32) and Eq. (33) respectively. The approximated solutions for fitness function (25) are calculated, and results for inputs between 0 and 1

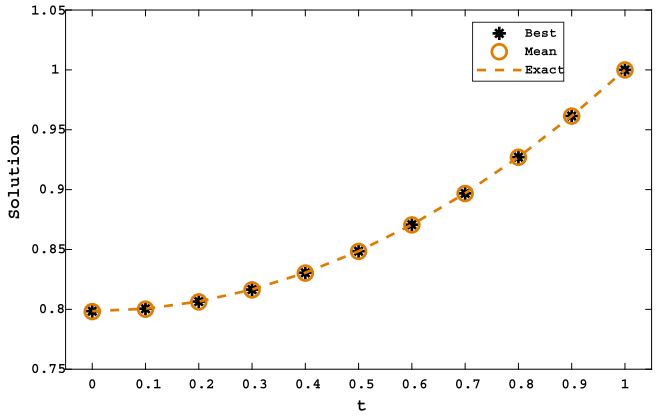

(a) Solution Graph.

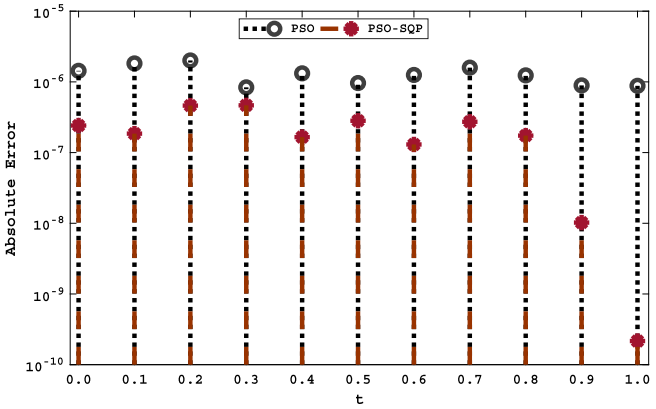

(b) Absolute Error Graph.

FIGURE 3. Case-I, approximate solution, and absolute error graphs.

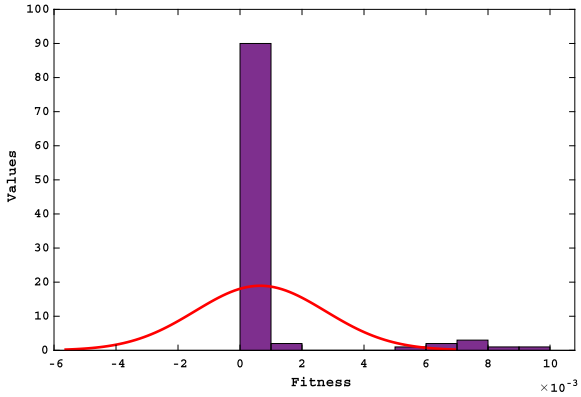

(a) Case-I FIT histogram.

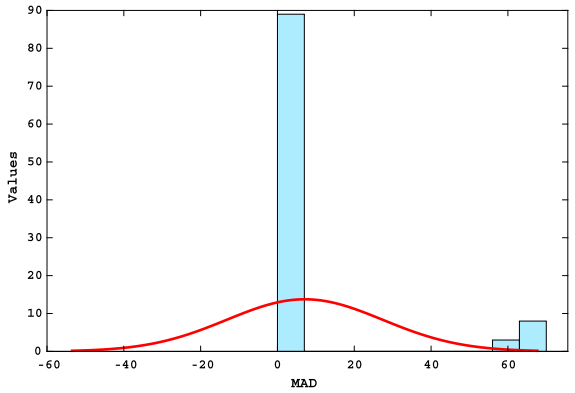

(b) Case-I MAD histogram.

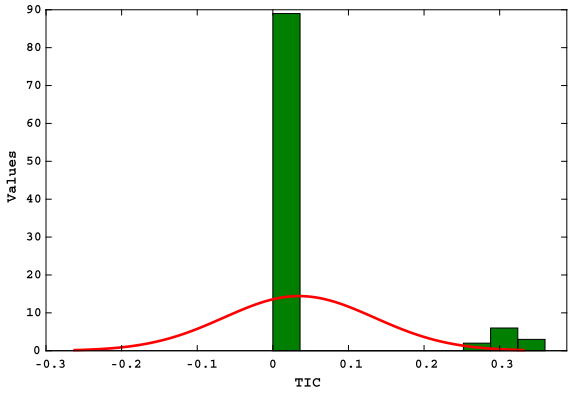

(c) Case-I TIC histogram.

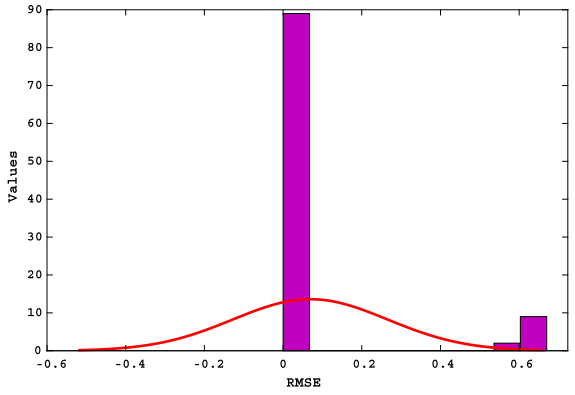

(d) Case-I RMSE histogram.

FIGURE 4. Histogram of FIT, MAD, TIC, RMSE, and ENSE for Cases I.

with h = 0.1 are shown graphically in Fig. (3) and numerically in Tab. (1). Furthermore, AEs are determined for PSO and PSO-SQP results, which are shown graphically in Fig. (3) and numerically in Tab. (2).

The data shown in Tab. (2) and Fig. (3) indicate that the PSO and PSO-SQP absolute errors are about 10^{-6} to 10^{-7} and 10^{-7} to 10^{-8} respectively, which means that PSO achieved $(6-7)$ and PSO-SQP achieved $(7-8)$ decimal places of precision from the reference results. The remaining techniques PS-AST, and GA-AST [9] absolute errors lie at around 10^{-5} and 10^{-6} respectively, which means that the PSO and PSO-SQP is relatively better and more effective than the rest of the techniques for this case of the reactive transport model.

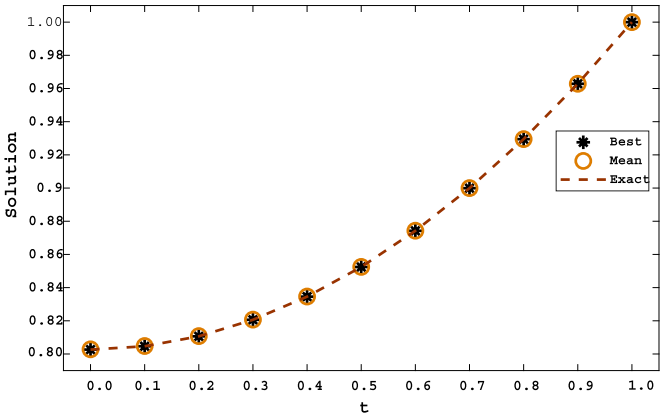

(a) Solution Graph.

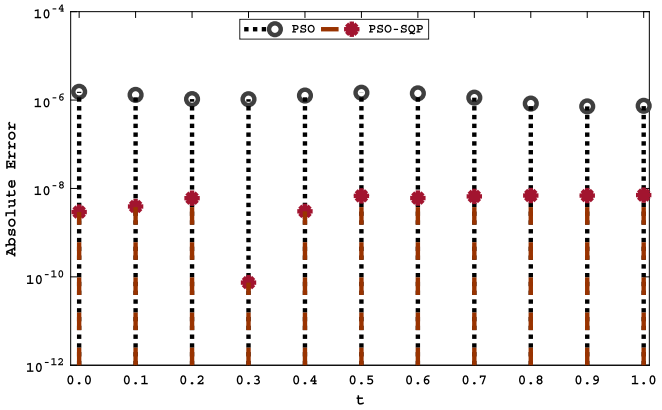

(b) Absolute Error Graph.

FIGURE 5. Case-II, approximate solution, and absolute error graphs.

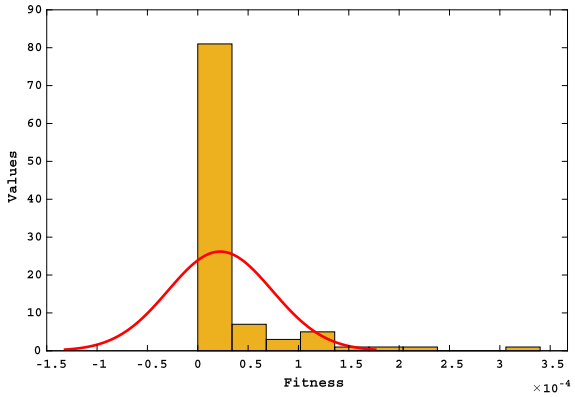

(a) Case-II FIT histogram.

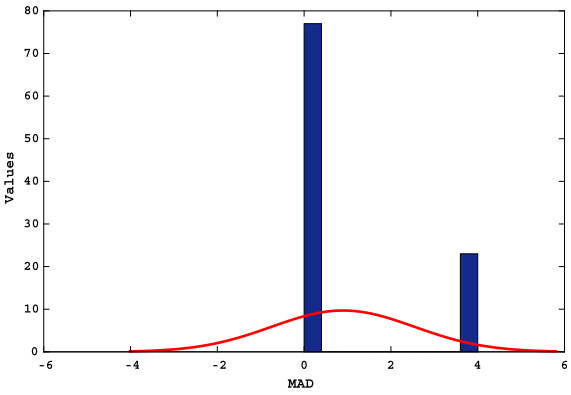

(b) Case-II MAD histogram.

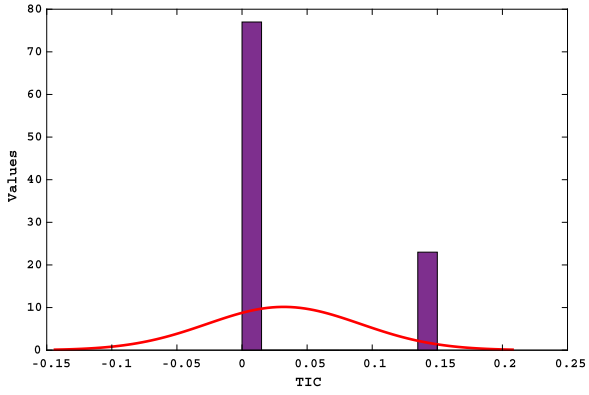

(c) Case-II TIC histogram.

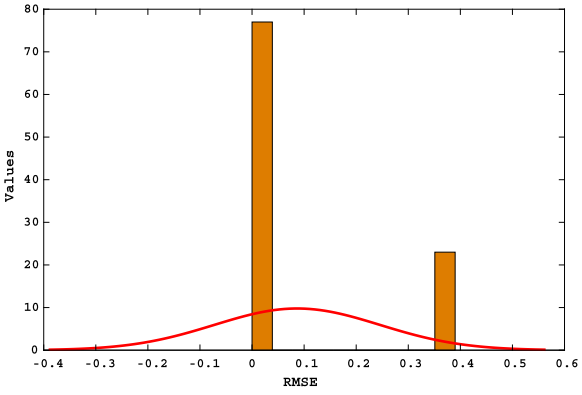

(d) Case-II RMSE histogram.

FIGURE 6. Histogram and Box plot of FIT, MAD, TIC, and RMSE for Cases II.

B. CASE 2: $\beta = 0.3$ AND $\alpha = -0.2$

The reactive transport model given in Eqs. (4,5) in this case can be written as [9]:

$$\frac{d^2\theta}{dx^2} - \frac{(0.3)\theta(x)}{(-0.2)+\theta(x)} = 0, \tag{26}$$

subject to the boundary condition

$$\frac{d\theta}{dx} = 0, \quad \theta(1) = 1. \tag{27}$$

The fitness function ε, for case 2 can be expressed as:

$$\varepsilon = \frac{1}{10}\sum_{k=1}^{10}\left(\frac{d^2\hat{\theta}_k}{dx^2} - \frac{0.3\hat{\theta}_k}{-0.2+\hat{\theta}_k}\right)^2 + \frac{1}{2}\left(\left(\hat{\theta}_K - 1\right)^2 + \left(\frac{d\theta_0}{dx}\right)^2\right). \tag{28}$$

PSO and PSO-SQP is applied for optimizing the fitness function (28). In Eq. (22), the optimal weights of PSO are

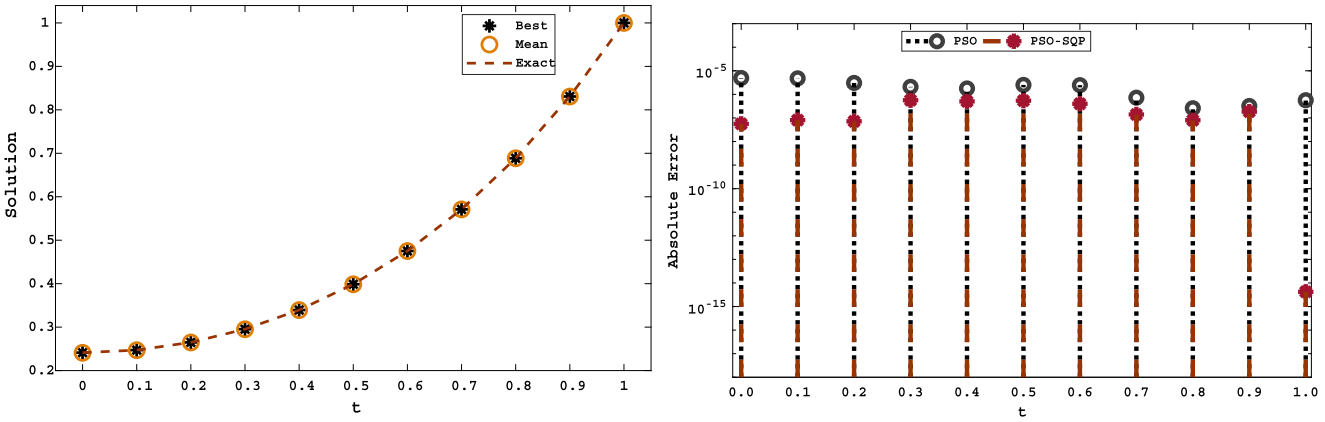

(a) Solution Graph. (b) Absolute Error Graph.

FIGURE 7. Case-III, approximate solution, and absolute error graphs.

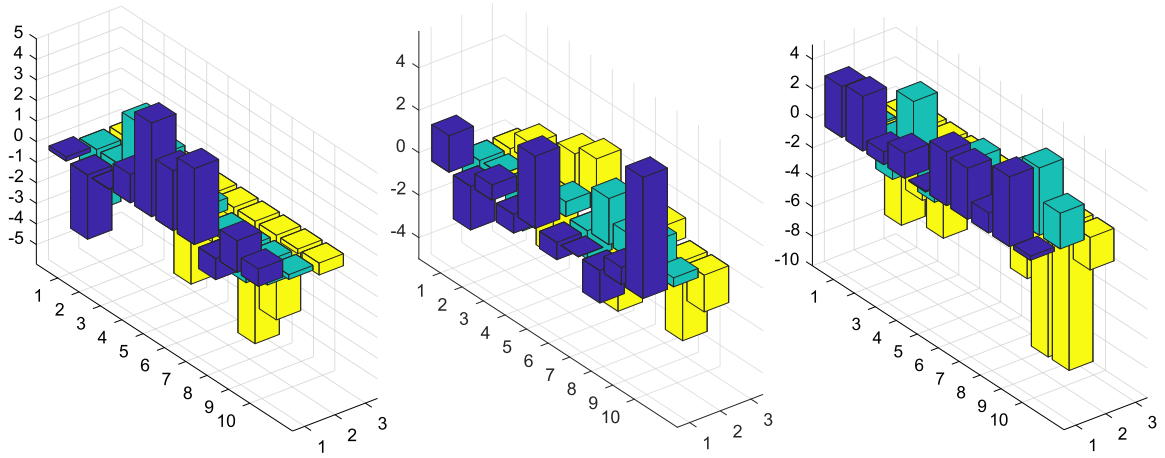

(a) Case-I Weights. (b) Case-II Weights. (c) Case-III Weights.

FIGURE 8. Graphs of weights for Cases I, II, III.

TABLE 2. Case 1, solution comparison of PSO and PSO-SQP with RK4.

Case I: $\beta = 0.5, \quad \alpha = 0.2$					
	Numerical				
x	RK4	PSO	PSO-SQP	GA-ASM	PS-ASM
0.0	0.798520	0.798521	0.798520	0.798479	0.798615
0.1	0.800519	0.800521	0.800520	0.800474	0.800607
0.2	0.806519	0.806521	0.806519	0.806477	0.806597
0.3	0.816527	0.816528	0.816527	0.816492	0.816594
0.4	0.830550	0.830551	0.830550	0.830525	0.830609
0.5	0.848604	0.848605	0.848604	0.848582	0.848653
0.6	0.870704	0.870705	0.870704	0.870682	0.870743
0.7	0.896870	0.896872	0.896870	0.896847	0.896900
0.8	0.927125	0.927126	0.927125	0.927103	0.927145
0.9	0.961493	0.961494	0.961493	0.961480	0.961503
1.0	1.000000	1.000001	1.000000	1.000000	1.000002

used to find the approximate solutions for case 2 of the reactive transport model as shown in Eq. (34) and Eq. (35) respectively. The estimated solutions for Eqs. (28) are calculated, and the results and AEs for inputs between 0 and 1 with

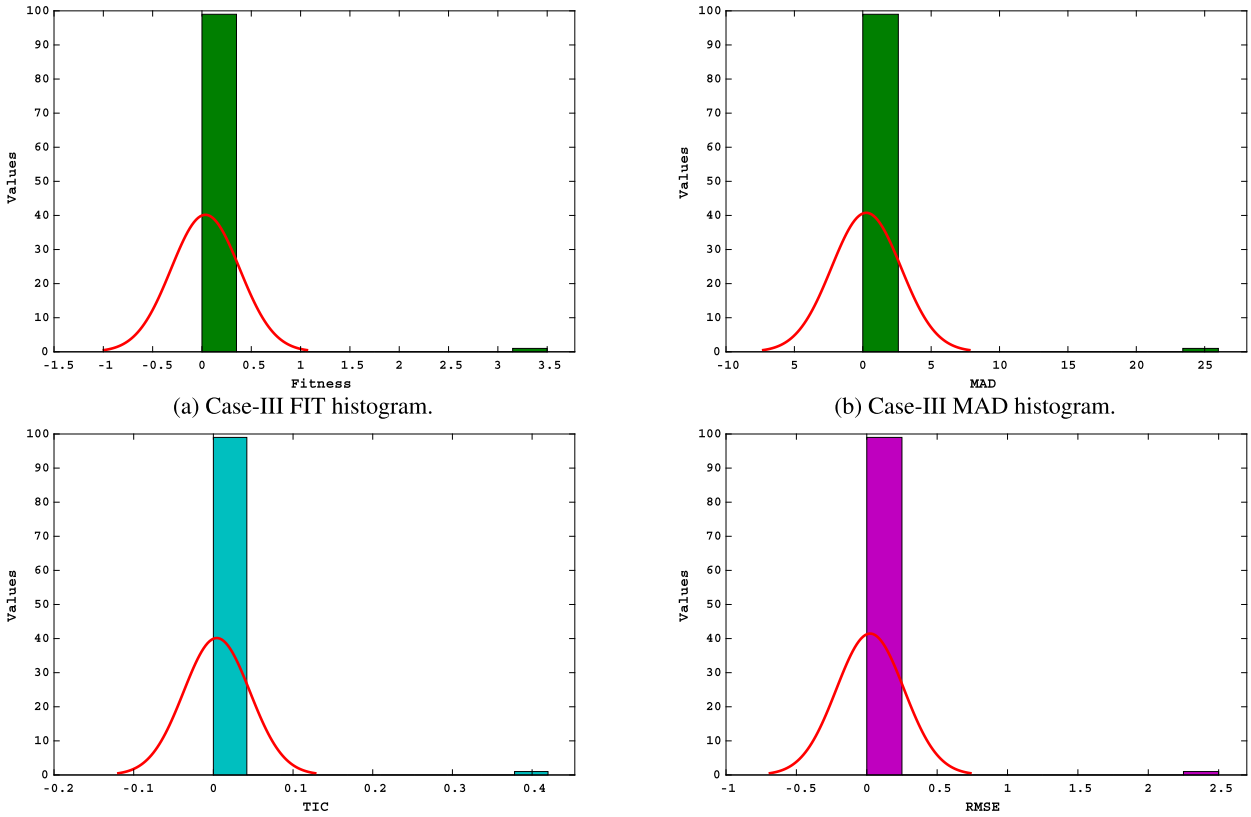

(a) Case-III FIT histogram.
(b) Case-III MAD histogram.
(c) Case-III TIC histogram.
(d) Case-III RMSE histogram.

FIGURE 9. Histogram and Box plot of FIT, MAD, TIC, and RMSE for Cases III.

TABLE 3. Case 1, PSO and PSO-SQP absolute error comparison.

Case I: $\beta = 0.5, \quad \alpha = 0.2$				
	Absolute Error			
x	PSO	PSO-SQP	GA-ASM	PS-ASM
0.0	1.43×10^{-6}	2.41×10^{-7}	1.75×10^{-5}	3.45×10^{-5}
0.1	1.82×10^{-6}	1.85×10^{-7}	1.72×10^{-5}	3.37×10^{-5}
0.2	2.01×10^{-6}	4.62×10^{-7}	1.52×10^{-5}	3.01×10^{-5}
0.3	8.37×10^{-7}	4.66×10^{-7}	1.29×10^{-5}	2.51×10^{-5}
0.4	1.32×10^{-6}	1.66×10^{-7}	9.64×10^{-6}	2.10×10^{-5}
0.5	9.63×10^{-7}	2.82×10^{-7}	7.84×10^{-6}	1.83×10^{-5}
0.6	1.25×10^{-6}	1.30×10^{-7}	6.37×10^{-6}	1.73×10^{-5}
0.7	1.59×10^{-6}	2.73×10^{-7}	5.11×10^{-6}	1.67×10^{-5}
0.8	1.24×10^{-6}	1.74×10^{-7}	4.15×10^{-6}	1.57×10^{-5}
0.9	8.92×10^{-7}	1.02×10^{-8}	2.91×10^{-6}	1.50×10^{-5}
1.0	8.80×10^{-7}	2.16×10^{-10}	1.03×10^{-6}	1.42×10^{-5}

h = 0.1 are shown graphically in Fig. (5) and numerically in Tab. (4), where the AEs are determined by comparing PSO and PSO-SQP results with RK4.

The data are shown in Tab. (4) and Fig. (5), which indicate that the PSO and PSO-SQP absolute errors are about 10^{-6} to 10^{-7}, and 10^{-9} to 10^{-11} respectively, which means that the PSO and PSO-SQP results are overlapping with the RK4 results. From Tab. (4) and Fig. (5) it is evident that the PSO-SQP model is better and more effective than PSO in this case of the reactive transport model.

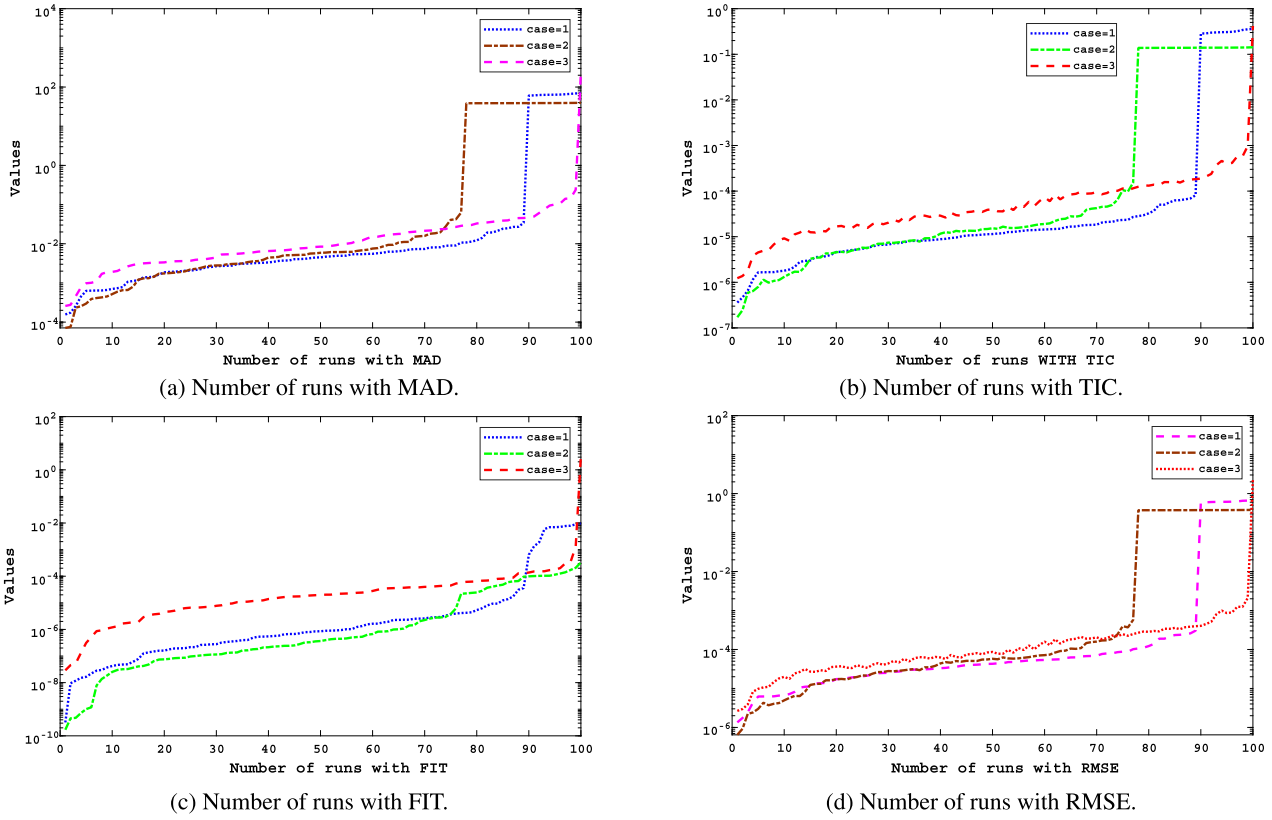

(a) Number of runs with MAD.

(b) Number of runs with TIC.

(c) Number of runs with FIT.

(d) Number of runs with RMSE.

FIGURE 10. Number of runs with MAD, TIC, FIT, and RNSE for Case-I, Case-II, Case-III.

TABLE 4. Case 2, numerical and absolute error comparison for PSO and PSO-SQP.

Case II: $\beta = 0.3, \quad \alpha = -0.2$					
	Numerical			Absolute Error	
x	RK4	PSO	PSO-SQP	PSO-AE	PSO-SQP-AE
0.0	0.802648942	0.802647404	0.802648945	1.54×10^{-6}	2.92×10^{-9}
0.1	0.804646469	0.804645159	0.804646472	1.31×10^{-6}	3.91×10^{-9}
0.2	0.810635772	0.810634721	0.810635777	1.05×10^{-6}	6.02×10^{-9}
0.3	0.820607160	0.820606116	0.820607160	1.04×10^{-6}	7.41×10^{-11}
0.4	0.834544886	0.834543621	0.834544883	1.26×10^{-6}	3.04×10^{-9}
0.5	0.852427781	0.852426316	0.852427775	1.46×10^{-6}	6.79×10^{-9}
0.6	0.874229996	0.874228579	0.874229990	1.41×10^{-6}	6.06×10^{-9}
0.7	0.899921872	0.899920739	0.899921866	1.13×10^{-6}	6.61×10^{-9}
0.8	0.929470815	0.929469983	0.929470809	8.32×10^{-7}	6.91×10^{-9}
0.9	0.962842168	0.962841449	0.962842161	7.19×10^{-7}	6.90×10^{-9}
1.0	1.000000007	0.999999266	1.000000000	7.41×10^{-7}	7.08×10^{-9}

C. CASE 3: $\beta = 6$ AND $\alpha = 1$

In this case the reactive transport model given in Eqs. (4,5) is written as [9]:

$$\frac{\mathrm{d}^2\theta}{\mathrm{d}x^2} - \frac{6\theta(x)}{1+\theta(x)} = 0, \tag{29}$$

subject to the boundary condition

$$\frac{\mathrm{d}\theta(0)}{\mathrm{d}x} = 0, \quad \theta(1) = 1. \tag{30}$$

The fitness function ε for case 3 can be expressed as:

$$\varepsilon = \frac{1}{10}\sum_{k=1}^{10}\left(\frac{\mathrm{d}^2\hat{\theta}_k}{\mathrm{d}x^2} - \frac{6\hat{\theta}_k}{1+\hat{\theta}_k}\right)^2 + \frac{1}{2}\left(\left(\hat{\theta}_K - 1\right)^2 + \left(\frac{\mathrm{d}\theta_0}{\mathrm{d}x}\right)^2\right). \tag{31}$$

PSO and PSO-SQP are used to optimize the fitness function (31). The optimal weights are used in Eq. (22), to find

TABLE 5. Case 3, solution comparison of PSO and PSO-SQP with RK4.

Case III: $\beta = 6, \quad \alpha = 1$					
	Numerical				
x	RK4	PSO	PSO-SQP	GA-ASM	PS-ASM
0.0	0.241272	0.241277	0.241272	0.241229	0.241230
0.1	0.247122	0.247127	0.247122	0.247083	0.247082
0.2	0.264899	0.264902	0.264899	0.264864	0.264865
0.3	0.295277	0.295279	0.295277	0.295244	0.295247
0.4	0.339368	0.339370	0.339368	0.339329	0.339339
0.5	0.398693	0.398696	0.398693	0.398657	0.398667
0.6	0.475148	0.475150	0.475148	0.475119	0.475123
0.7	0.570951	0.570952	0.570951	0.570925	0.570925
0.8	0.688575	0.688575	0.688575	0.688540	0.688545
0.9	0.830674	0.830674	0.830674	0.830627	0.830637
1.0	1.000000	0.999999	1.000000	0.999953	0.999963

TABLE 6. Case 3, PSO and PSO-SQP absolute error comparison.

Case III: $\beta = 6, \quad \alpha = 1$				
	Absolute Error			
t	PSO	PSO-SQP	GA-ASM	PS-ASM
0.0	4.95×10^{-6}	5.60×10^{-8}	5.89×10^{-5}	9.52×10^{-5}
0.1	4.78×10^{-6}	8.10×10^{-8}	5.31×10^{-5}	8.56×10^{-5}
0.2	3.06×10^{-6}	7.18×10^{-8}	3.91×10^{-5}	6.91×10^{-5}
0.3	2.09×10^{-6}	5.65×10^{-7}	3.66×10^{-5}	5.72×10^{-5}
0.4	1.78×10^{-6}	5.04×10^{-7}	4.09×10^{-5}	5.12×10^{-5}
0.5	2.52×10^{-6}	5.39×10^{-7}	3.96×10^{-5}	4.88×10^{-5}
0.6	2.46×10^{-6}	3.99×10^{-7}	3.42×10^{-5}	4.79×10^{-5}
0.7	7.23×10^{-7}	1.40×10^{-7}	3.43×10^{-5}	4.96×10^{-5}
0.8	2.58×10^{-7}	7.99×10^{-8}	4.21×10^{-5}	5.31×10^{-5}
0.9	3.21×10^{-7}	1.85×10^{-7}	5.38×10^{-5}	5.94×10^{-5}
1.0	5.65×10^{-7}	4.22×10^{15}	5.85×10^{-5}	6.35×10^{-5}

TABLE 7. Acronyms used in this paper.

Acronyms	Full form	Acronyms	Full form
ANNs	Artificial neural networks	**PSO**	Particle Swarm Optimization
ASA	Active Set Algorithm	**MAD**	Mean absolute deviation
RTM	Reactive Transport Model	**RMSE**	Root-mean-square error
AE	Absolute error	**TIC**	inequality coefficient of Theil
IPT	Interior Point Technique	**RKM**	Runge Kutta Method
GA	Genetic Algorithm	**AE**	Absolute Error
SQP	Sequential Quadratic Programming	**NNs**	Neural Networks
V	Velocity of Particle	**f**	Activation function (Log-sigmiod)

the approximate solutions for case 3 of the reactive transport model, as shown in Eq. (32) and Eq. (33) respectively. The approximated solutions for Eqs. (31) are calculated, and results for inputs between 0 and 1 with h = 0.1 are graphically

represented in Fig. (7) and numerically in Tab. (4). In addition, AEs are determined for PSO, and PSO-SQP results, which are graphically illustrated in Fig. (7) and numerically in Tab. (5).

The absolute errors of PSO and PSO-SQP are about 10^{-6} to 10^{-7} and 10^{-7} to 10^{-8} respectively, as shown in Tab. (6), implying that PSO and PSO-SQP achieve (6-7) and (7-8) decimal places of precision from the reference results. The absolute errors of the remaining techniques, GA, PS-AST, and GA-AST [9] are around 10^{-4} to 10^{-5}, indicating that the PSO and PSO-SQP are better and more effective than the other techniques for this case of the reactive transport model.

VII. CONCLUSION

The following conclusions are summarized:

The steady-state reaction-diffusion model that occurs in the studies of soft-tissues and microvessels in the fluid and solvent transport models is discussed using the approximation ability of ANN modeling via the heuristic technique. The PSO and PSO-SQP computational methodologies can investigate various cases of reaction-diffusion models by varying the half-saturation concentration rate and the characteristic reaction rate with reasonable precision. In Case I, the proposed technique show good agreement with RK4 by achieving an accuracy of 10^{-8}. In Case II, we compared the results to an RK4 solution, demonstrating that the proposed technique achieves an accuracy of 10^{-11}. In Case III, the accuracy for the proposed approach is also up to 10^{-15}, which is a good approximation for the RTM model. Comparing the proposed method to RK4 and other numerical methods shows that the PSO and PSO-SQP performance for all cases of the reaction-diffusion model is better than the other methods.

For all three cases, histograms for the performance indicator and fitness function are shown in Figs. (4), (6), and (9) respectively. Similarly number of independent runs of MAD, TIC, FIT and RMSE are also done for reactive transport model as shown in Fig.(10). MAD values show that the majority are close to zero in Fig. (10a), TIC values show that more than 90% of the values are less than or equal to 10^{-03} in Fig. (10b), and RMSE values show that more than 90% of the values are less than or equal to 10^{-03} in Fig. (10d) in all three cases. Similarly, for all three cases the fitness (FIT) values in Fig. (10c) show that more than 90% of the values are less than or equal to 10^{-03}. The preceding discussion validates the PSO-SQP algorithm's effectiveness in investigating the proposed model.

APPENDIX

$$\begin{aligned}\hat{\theta}_{PSO_1} &= \frac{0.2021}{1+e^{-(1.7705\,t-5.9492)}} + \frac{-2.9715}{1+e^{-(-5.0838\,t-1.0300)}} \\ &+ \frac{-2.7157}{1+e^{-(4.5532\,t-1.7435)}} + \frac{-3.1211}{1+e^{-(-0.8215\,t-4.1161)}} \\ &+ \frac{-0.5007}{1+e^{-(-2.3513\,t+1.5383)}} + \frac{0.1687}{1+e^{-(2.9211\,t-1.1782)}} \\ &+ \frac{-0.0174}{1+e^{-(0.5851\,t-0.2223)}} + \frac{2.6221}{1+e^{-(-0.5099\,t+0.8405)}} \\ &+ \frac{-2.2349}{1+e^{-(3.6930\,t-0.2313)}} + \frac{1.3796}{1+e^{-(-0.3855\,t-0.5792)}}. \end{aligned} \tag{32}$$

$$\begin{aligned}\hat{\theta}_{PSO-SPQ_1} &= \frac{-2.4736}{1+e^{-(-0.8882\,t-6.0781)}} + \frac{5.58693}{1+e^{-(-3.2511\,t-29.999)}} \\ &+ \frac{5.67261}{1+e^{-(23.4867\,t-1.8893)}} + \frac{7.99743}{1+e^{-(-1.0701\,t-7.0334)}} \\ &+ \frac{-7.1831}{1+e^{-(4.77724\,t-29.999)}} + \frac{-8.5775}{1+e^{-(22.0975\,t-0.8985)}} \\ &+ \frac{26.5423}{1+e^{-(0.90005\,t+5.0501)}} + \frac{0.78362}{1+e^{-(-6.5910\,t+9.0472)}} \\ &+ \frac{-4.1526}{1+e^{-(-29.994\,t+6.0712)}} + \frac{10.6149}{1+e^{-(0.18647\,t+6.9488)}}. \end{aligned} \tag{33}$$

$$\begin{aligned}\hat{\theta}_{PSO_2} &= \frac{1.7221}{1+e^{-(-0.1316\,t-0.6687)}} + \frac{-1.2043}{1+e^{-(1.7413\,t-1.5284)}} \\ &+ \frac{-2.1761}{1+e^{-(3.3977\,t+1.1231)}} + \frac{-2.0576}{1+e^{-(0.7003\,t+0.9381)}} \\ &+ \frac{0.0115}{1+e^{-(2.16804\,t+0.8088)}} + \frac{0.8665}{1+e^{-(-0.8133\,t+1.4451)}} \\ &+ \frac{0.7252}{1+e^{-(-1.3317\,t+-3.7527)}} + \frac{-1.9923}{1+e^{-(-4.3468\,t+5.7095)}} \\ &+ \frac{-3.7246}{1+e^{-(-0.0173\,t+0.4250)}} + \frac{-0.8833}{1+e^{-(2.17707\,t-1.7331)}}. \end{aligned} \tag{34}$$

$$\begin{aligned}\hat{\theta}_{PSO_SQP_2} &= \frac{10.1703}{1+e^{-(1.75216\,t-2.8503)}} + \frac{-1.3529}{1+e^{-(-7.1086\,t+29.938)}} \\ &+ \frac{4.29177}{1+e^{-(-8.9599\,t-1.0190)}} + \frac{27.0962}{1+e^{-(-1.9197\,t-3.9968)}} \\ &+ \frac{3.02388}{1+e^{-(-4.0383\,t-14.427)}} + \frac{7.02808}{1+e^{-(27.0248\,t-0.7100)}} \\ &+ \frac{3.09180}{1+e^{-(0.8776t+4.1699)}} + \frac{-2.7761}{1+e^{-(-4.3606\,t-25.888)}} \\ &+ \frac{7.94666}{1+e^{-(-2.1567\,t-25.888)}} + \frac{29.0625}{1+e^{-(-0.4797\,t+5.9041)}}. \end{aligned} \tag{35}$$

$$\begin{aligned}\hat{\theta}_{PSO_3} &= \frac{3.4418}{1+e^{-(-2.4031t-5.5774)}} + \frac{-0.1426}{1+e^{-(-3.1278\,t+1.3603)}} \\ &+ \frac{-7.5151}{1+e^{-(0.0817\,t+3.1149)}} + \frac{3.6964}{1+e^{-(-0.4584\,t-9.9571)}} \\ &+ \frac{-2.7033}{1+e^{-(-1.3053t+4.7346)}} + \frac{-4.9003}{1+e^{-(3.6486\,t+4.5602)}} \\ &+ \frac{0.8744}{1+e^{-(2.4451\,t-9.9457)}} + \frac{3.5093}{1+e^{-(-3.7887\,t+0.2812)}} \\ &+ \frac{-6.5408}{1+e^{-(3.4582\,t+2.4186)}} + \frac{1.7018}{1+e^{-(-1.1719\,t-2.2046)}}. \end{aligned} \tag{36}$$

$$\hat{\theta}_{PSO_SQP_3} = \frac{11.4590}{1+e^{-(-2.7594\,t-1.6726)}} + \frac{2.75847}{1+e^{-(-2.5502\,t+14.6979)}}$$

$$+\frac{-6.5859}{1+e^{-(-25.082\ t-16.6476)}}+\frac{-6.2284}{1+e^{-(-2.3489\ t-28.5611)}}+\frac{3.54573}{1+e^{-(-2.6961\ t-17.9642)}}+\frac{-9.0767}{1+e^{-(-0.6952\ t-0.3231)}}+\frac{3.89313}{1+e^{-(-4.4020\ t-2.9078)}}+\frac{1.98443}{1+e^{-(-1.8959\ t+11.2061)}}+\frac{-3.1188}{1+e^{-(0.14143\ t-0.9077)}}+\frac{17.7826}{1+e^{-(-5.0960\ t-1.9818)}}. \quad (37)$$

REFERENCES

[1] E. Shivanian, "On the multiplicity of solutions of the nonlinear reactive transport model," *Ain Shams Eng. J.*, vol. 5, no. 2, pp. 637–645, Jun. 2014.

[2] H. Vosoughi, E. Shivanian, and S. Abbasbandy, "Unique and multiple PHAM series solutions of a class of nonlinear reactive transport model," *Numer. Algorithms*, vol. 61, no. 3, pp. 515–524, Nov. 2012.

[3] A. J. Ellery and M. J. Simpson, "An analytical method to solve a general class of nonlinear reactive transport models," *Chem. Eng. J.*, vol. 169, nos. 1–3, pp. 313–318, May 2011.

[4] C. Steefel, D. Depaolo, and P. Lichtner, "Reactive transport modeling: An essential tool and a new research approach for the earth sciences," *Earth Planet. Sci. Lett.*, vol. 240, nos. 3–4, pp. 539–558, Dec. 2005.

[5] K. T. B. MacQuarrie and K. U. Mayer, "Reactive transport modeling in fractured rock: A state-of-the-science review," *Earth-Sci. Rev.*, vol. 72, nos. 3–4, pp. 189–227, Oct. 2005.

[6] T. Pabst, J. Molson, M. Aubertin, and B. Bussière, "Reactive transport modelling of the hydro-geochemical behaviour of partially oxidized acid-generating mine tailings with a monolayer cover," *Appl. Geochemistry*, vol. 78, pp. 219–233, Mar. 2017.

[7] P. Regnier, P. Jourabchi, and C. P. Slomp, "Reactive-transport modeling as a technique for understanding coupled biogeochemical processes in surface and subsurface environments," *Netherlands J. Geosci. - Geologie en Mijnbouw*, vol. 82, no. 1, pp. 5–18, Apr. 2003.

[8] J. Vilcáez, L. Li, D. Wu, and S. S. Hubbard, "Reactive transport modeling of induced selective plugging byLeuconostoc mesenteroidesin carbonate formations," *Geomicrobiol. J.*, vol. 30, no. 9, pp. 813–828, Oct. 2013.

[9] I. Ahmad, H. Ilyas, A. Urooj, M. S. Aslam, M. Shoaib, and M. A. Z. Raja, "Novel applications of intelligent computing paradigms for the analysis of nonlinear reactive transport model of the fluid in soft tissues and microvessels," *Neural Comput. Appl.*, vol. 31, no. 12, pp. 9041–9059, 2019.

[10] S. Abbasbandy, "Approximate solution for the nonlinear model of diffusion and reaction in porous catalysts by means of the homotopy analysis method," *Chem. Eng. J.*, vol. 136, nos. 2–3, pp. 144–150, Mar. 2008.

[11] S. Abbasbandy, E. Magyari, and E. Shivanian, "The homotopy analysis method for multiple solutions of nonlinear boundary value problems," *Commun. Nonlinear Sci. Numer. Simul.*, vol. 14, nos. 9–10, pp. 3530–3536, Sep. 2009.

[12] Y.-P. Sun, S.-B. Liu, and S. Keith, "Approximate solution for the nonlinear model of diffusion and reaction in porous catalysts by the decomposition method," *Chem. Eng. J.*, vol. 102, no. 1, pp. 1–10, Aug. 2004.

[13] T. P. Clement, Y. Sun, B. S. Hooker, and J. N. Petersen, "Modeling multispecies reactive transport in ground water," *Groundwater Monitor. Remediation*, vol. 18, no. 2, pp. 79–92, May 1998.

[14] J. E. Bailey and D. F. Ollis, *Biochemical Engineering Fundamentals*. New York, NY, USA: McGraw-Hill, 2018.

[15] C. Zheng and G. D. Bennett, *Applied Contaminant Transport Modeling*, vol. 2. Hoboken, NJ, USA: Wiley, 2002.

[16] N. R. Amundson, "Theory of catalysis: The mathematical theory of diffusion and reaction in permeable catalysts. Rutherford aris. Clarendon (Oxford University Press), New York, 1975. Two volumes vol. 1, the theory of the steady state. xvi, 444 pp., illus. 39.50. Vol. 2, questions of uniqueness, stability, and transient behaviour. xiv, 218 pp., illus. 25.75," *Science*, vol. 190, no. 4215, pp. 667–668, 1975.

[17] R. E. West, "Material and energy balance computations. EJ Henley and EM Rosen," *Chem. Eng. Educ.*, vol. 5, no. 2, pp. 98–99, 1971.

[18] M. T. Van Genuchten, *Analytical Solutions of the One-Dimensional Convective-Dispersive Solute Transport Equation*, no. 1661. Annapolis, MA, USA: U.S. Department of Agriculture, Agricultural Research Service, 1982.

[19] M. T. V. Genuchten, F. J. Leij, T. H. Skaggs, N. Toride, S. A. Bradford, and E. M. Pontedeiro, "Exact analytical solutions for contaminant transport in rivers 1. The equilibrium advection-dispersion equation," *J. Hydrol. Hydromechanics*, vol. 61, no. 2, pp. 146–160, Jun. 2013.

[20] D. Kuzmin, "A guide to numerical methods for transport equations," Univ. Erlangen-Nuremberg, Erlangen, Germany, Tech. Rep., 2010, p. 24.

[21] A.-M. Wazwaz, R. Rach, and L. Bougoffa, "Dual solutions for nonlinear boundary value problems by the adomian decomposition method," *Int. J. Numer. Methods Heat Fluid Flow*, vol. 26, no. 8, pp. 2393–2409, Nov. 2016.

[22] M. M. Miah, H. M. S. Ali, M. A. Akbar, and A. M. Wazwaz, "Some applications of the (G'/G, 1/G)-expansion method to find new exact solutions of NLEEs," *Eur. Phys. J. Plus*, vol. 132, no. 6, pp. 1–15, Jun. 2017.

[23] R. Rach, J.-S. Duan, and A.-M. Wazwaz, "On the solution of non-isothermal reaction-diffusion model equations in a spherical catalyst by the modified adomian method," *Chem. Eng. Commun.*, vol. 202, no. 8, pp. 1081–1088, Aug. 2015.

[24] A.-M. Wazwaz, R. Rach, and J.-S. Duan, "A study on the systems of the Volterra integral forms of the Lane–Emden equations by the adomian decomposition method," *Math. Methods Appl. Sci.*, vol. 37, no. 1, pp. 10–19, Jan. 2014.

[25] J. Donea, "A Taylor–Galerkin method for convective transport problems," *Int. J. Numer. Methods Eng.*, vol. 20, no. 1, pp. 101–119, Jan. 1984.

[26] M. Al-Smadi and O. A. Arqub, "Computational algorithm for solving Fredholm time-fractional partial integrodifferential equations of Dirichlet functions type with error estimates," *Appl. Math. Comput.*, vol. 342, pp. 280–294, Feb. 2019.

[27] Z. Abo-Hammour, O. A. Arqub, S. Momani, and N. Shawagfeh, "Optimization solution of Troesch's and Bratu's problems of ordinary type using novel continuous genetic algorithm," *Discrete Dyn. Nature Soc.*, vol. 2014, pp. 1–15, Jan. 2014.

[28] O. A. Arqub and B. Maayah, "Numerical solutions of integrodifferential equations of Fredholm operator type in the sense of the Atangana–Baleanu fractional operator," *Chaos, Solitons Fractals*, vol. 117, pp. 117–124, Dec. 2018.

[29] H. MolaAbasi and I. Shooshpasha, "Prediction of zeolite-cement-sand unconfined compressive strength using polynomial neural network," *Eur. Phys. J. Plus*, vol. 131, no. 4, p. 108, Apr. 2016.

[30] P. Bénilan and H. Brezis, "Nonlinear problems related to the Thomas-Fermi equation," *J. Evol. Equ.*, vol. 3, no. 4, pp. 673–770, Dec. 2003.

[31] W. Waseem, M. Sulaiman, A. Alhindi, and H. Alhakami, "A soft computing approach based on fractional order dpso algorithm designed to solve the corneal model for eye surgery," *IEEE Access*, vol. 8, pp. 61576–61592, 2020.

[32] N. A. Khan, M. Sulaiman, A. J. Aljohani, P. Kumam, and H. Alrabaiah, "Analysis of multi-phase flow through porous media for imbibition phenomena by using the LeNN-WOA-NM algorithm," *IEEE Access*, vol. 8, pp. 196425–196458, 2020.

[33] W. Huang, T. Jiang, X. Zhang, N. A. Khan, and M. Sulaiman, "Analysis of beam-column designs by varying axial load with internal forces and bending rigidity using a new soft computing technique," *Complexity*, vol. 2021, pp. 1–19, Mar. 2021.

[34] M. Sulaiman, A. Ahmad, A. Khan, and S. Muhammad, "Hybridized symbiotic organism search algorithm for the optimal operation of directional overcurrent relays," *Complexity*, vol. 2018, pp. 1–11, Jan. 2018.

[35] E. Slikboer, P. Viegas, Z. Bonaventura, E. Garcia-Caurel, A. Sobota, A. Bourdon, and O. Guaitella, "Experimental and numerical investigation of the transient charging of a dielectric surface exposed to a plasma jet," *Plasma Sour. Sci. Technol.*, vol. 28, no. 9, Sep. 2019, Art. no. 095016.

[36] A. Ahmad, M. Sulaiman, A. J. Aljohani, A. Alhindi, and H. Alrabaiah, "Design of an efficient algorithm for solution of bratu differential equations," *Ain Shams Eng. J.*, vol. 12, no. 2, pp. 2211–2225, Jun. 2021.

[37] T. Ji and J. Hou, "Numerical solution of the Bagley–Torvik equation using Laguerre polynomials," *SeMA J.*, vol. 77, no. 1, pp. 97–106, Mar. 2020.

[38] I. Ahmad, O. Bazighifan, A. Abouelregal, and H. Ahmad, "Multistage optimal homotopy asymptotic method for the nonlinear Riccati ordinary differential equation in nonlinear physics," *Appl. Math. Inf. Sci.*, vol. 14, no. 6, pp. 1–7, Jan. 2020.

[39] A. Sadeghi, H. Hassanzadeh, T. G. Harding, B. MacFarlane, S. Bashti, and P. Haghighat, "Numerical modeling of electromagnetic-based thermal recovery techniques combined with solvent injection," *Int. J. Heat Mass Transf.*, vol. 151, Apr. 2020, Art. no. 119393.

[40] A. Liljenberg, "Spherically symmetric self-gravitating elastic bodies: A numerical investigation," Tech. Rep., 2020.

[41] A. M. Hemeida, A. S. Omer, A. M. Bahaa-Eldin, S. Alkhalaf, M. Ahmed, T. Senjyu, and G. El-Saady, "Multi-objective multi-verse optimization of renewable energy sources-based micro-grid system: Real case," *Ain Shams Eng. J.*, vol. 13, no. 1, Jan. 2022, Art. no. 101543.
[42] R. G. Ayestarán, "Fast near-field multifocusing of antenna arrays including element coupling using neural networks," *IEEE Antennas Wireless Propag. Lett.*, vol. 17, no. 7, pp. 1233–1237, Jul. 2018.
[43] J. G. Berryman and C. J. Holland, "Nonlinear diffusion problem arising in plasma physics," *Phys. Rev. Lett.*, vol. 40, no. 26, p. 1720, 1978.
[44] C. R. Rodríguez, S. C. Figueiredo, M. Deprez, D. Snoeck, E. Schlangen, and B. Šavija, "Numerical investigation of crack self-sealing in cement-based composites with superabsorbent polymers," *Cement Concrete Composites*, vol. 104, Nov. 2019, Art. no. 103395.
[45] A. Weiner, J. Timmermann, C. Pesci, J. Grewe, M. Hoffmann, M. Schlüter, and D. Bothe, "Experimental and numerical investigation of reactive species transport around a small rising bubble," *Chem. Eng. Sci., X*, vol. 1, Feb. 2019, Art. no. 100007.
[46] Y. Shi and R. C. Eberhart, "Empirical study of particle swarm optimization," in *Proc. Congr. Evol. Comput.*, Washington, DC, USA, vol. 3, Jul. 1999, pp. 1945–1950.
[47] A. P. Engelbrecht, *Computational Intelligence: An Introduction*. Hoboken, NJ, USA: Wiley, 2007.
[48] R. Toushmalani, "Gravity inversion of a fault by particle swarm optimization (PSO)," *SpringerPlus*, vol. 2, no. 1, p. 315, Dec. 2013.
[49] M. Shen, Z.-H. Zhan, W.-N. Chen, Y.-J. Gong, J. Zhang, and Y. Li, "Bi-velocity discrete particle swarm optimization and its application to multicast routing problem in communication networks," *IEEE Trans. Ind. Electron.*, vol. 61, no. 12, pp. 7141–7151, Dec. 2014.
[50] A. Khare and S. Rangnekar, "A review of particle swarm optimization and its applications in solar photovoltaic system," *Appl. Soft Comput.*, vol. 13, no. 5, pp. 2997–3006, May 2013.
[51] J. Soares, T. Sousa, H. Morais, Z. Vale, B. Canizes, and A. Silva, "Application-specific modified particle swarm optimization for energy resource scheduling considering vehicle-to-grid," *Appl. Soft Comput.*, vol. 13, no. 11, pp. 4264–4280, 2013.
[52] A. A. A. Esmin, R. A. Coelho, and S. Matwin, "A review on particle swarm optimization algorithm and its variants to clustering high-dimensional data," *Artif. Intell. Rev.*, vol. 44, no. 1, pp. 23–45, 2015.
[53] K. B. Lee and J. H. Kim, "Multiobjective particle swarm optimization with preference-based sort and its application to path following footstep optimization for humanoid robots," *IEEE Trans. Evol. Comput.*, vol. 17, no. 6, pp. 755–766, Dec. 2013.
[54] B. Akay, "A study on particle swarm optimization and artificial bee colony algorithms for multilevel thresholding," *Appl. Soft Comput.*, vol. 13, no. 6, pp. 3066–3091, 2013.
[55] E. Alba, J. Garcia-Nieto, L. Jourdan, and E.-G. Talbi, "Gene selection in cancer classification using PSO/SVM and GA/SVM hybrid algorithms," in *Proc. IEEE Congr. Evol. Comput.*, Sep. 2007, pp. 284–290.
[56] H. Liao, W. Wu, and D. Fang, "The reduced space sequential quadratic programming (SQP) method for calculating the worst resonance response of nonlinear systems," *J. Sound Vib.*, vol. 425, pp. 301–323, Jul. 2018.
[57] R. Fletcher, *Practical Methods of Optimization*. Hoboken, NJ, USA: Wiley, 2013.
[58] K. Schittkowski, "NLPQL: A FORTRAN subroutine solving constrained nonlinear programming problems," *Ann. Oper. Res.*, vol. 5, no. 2, pp. 485–500, Jun. 1986.
[59] O. D. Montoya, W. Gil-González, and A. Garces, "Sequential quadratic programming models for solving the OPF problem in DC grids," *Electr. Power Syst. Res.*, vol. 169, pp. 18–23, Apr. 2019.
[60] Y. Kim, P. Carbonetto, M. Stephens, and M. Anitescu, "A fast algorithm for maximum likelihood estimation of mixture proportions using sequential quadratic programming," *J. Comput. Graph. Statist.*, vol. 29, no. 2, pp. 261–273, Apr. 2020.
[61] A. Witkowska and R. Śmierzchalski, "Adaptive dynamic control allocation for dynamic positioning of marine vessel based on backstepping method and sequential quadratic programming," *Ocean Eng.*, vol. 163, pp. 570–582, Sep. 2018.
[62] D. Kouzoupis, G. Frison, A. Zanelli, and M. Diehl, "Recent advances in quadratic programming algorithms for nonlinear model predictive control," *Vietnam J. Math.*, vol. 46, no. 4, pp. 863–882, Dec. 2018.
[63] Y. Welhazi, T. Guesmi, B. M. Alshammari, K. Alqunun, A. Alateeq, Y. Almalaq, R. Alsabhan, and H. H. Abdallah, "A novel hybrid chaotic Jaya and sequential quadratic programming method for robust design of power system stabilizers and static VAR compensator," *Energies*, vol. 15, no. 3, p. 860, Jan. 2022.

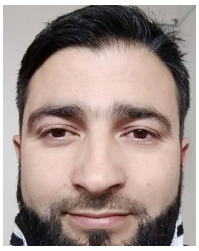

ABDUL HAMID GANIE received the M.Sc. degree from the University of Kashmir and the M.Phil. and Ph.D. degrees from the National Institute of Technology Srinagar, in 2014. He worked as a C. Lecturer at GDC Kupwara (2006), GDC Baramulla (2007), GDC Bandipora (2008), and NIT Srinagar (2011 and 2014), and later joined as an Assistant Professor at SSM College of Engineering and Technology, Pattan, in 2015. He has been working as an Assistant Professor at Saudi Electronic University, since 2018. He has published over 45 international publications. He is the author of two books *Tase of Matrix Methods* (Scholars Press) and *Taste of Cubic Equations and Fourier Series* (Generis Publishing).

IRFAN UR RAHMAN received the M.Phil. degree in applied mathematics from Abdul Wali Khan University Mardan, Pakistan, in 2020, where he is currently pursuing the Ph.D. degree. His research interests include mathematical optimization techniques, real world problems, heuristics, metaheuristics, multi-objective optimization, and design engineering optimization problems. He has the potential to accept any challenging environment in research productivity.

MUHAMMAD SULAIMAN received the B.Sc. degree from the University of Peshawar, in 2004, the M.Sc. and M.Phil. degrees in mathematics from Quaid-e-Azam University, Islamabad, Pakistan, in 2007 and 2009, respectively, and the Ph.D. degree in mathematics from the University of Essex, U.K., in 2015. From 2009 to 2016, he was a Lecturer in mathematics with Abdul Wali Khan University Mardan, Pakistan. From February 2016 to August 2021, he was an Assistant Professor with the Department of Mathematics, Abdul Wali Khan University Mardan, where he has been working as an Associate Professor of mathematics, since August 2021. He is the author of two book chapters and more than 59 research articles. His research interests include mathematical optimization techniques, global optimization, and evolutionary algorithms, heuristics, metaheuristics, multi-objective optimization, design engineering optimization problems, structural engineering optimization problems, linear programming, linear and non-linear least squares optimization problems, evolutionary algorithms, nature-inspired metaheuristics, artificial neural networks, and differential equations. He is an Associate Editor of the journal *COJ Reviews and Research* and *SCIREA Journal of Mathematics*.

KAMSING NONLAOPON received the B.S. degree in mathematics from Khon Kaen University, Khon Kaen, Thailand, in 2000, and the Ph.D. degree in mathematics from Chiang Mai University, Chiang Mai, Thailand, in 2005. He is currently an Associate Professor with the Department of Mathematics, Faculty of Science, Khon Kaen University. He has authored or coauthored more than 100 international peer-reviewed journals. His main research interests include differential equations, fluid dynamics, fractional calculus, generalized functions, inequalities and applications, mathematical model, quantum calculus, and special functions.